Key Factors Limiting Carbon Nanotube Yarn Strength: Exploring Processing-Structure-Property Relationships

Allison M. Beese,[†,‡] Xiaoding Wei,[†] Sourangsu Sarkar,[§] Rajaprakash Ramachandramoorthy,[†] Michael R. Roenbeck,[†] Alexander Moravsky,[∥] Matthew Ford,[†] Fazel Yavari,[†] Denis T. Keane,[⊥,#] Raouf O. Loutfy,[∥] SonBinh T. Nguyen,[§] and Horacio D. Espinosa*[,†]

[†]Department of Mechanical Engineering, Northwestern University, 2145 Sheridan Road, Evanston, Illinois 60208-3111, United States, [‡]Department of Materials Science and Engineering, Pennsylvania State University, University Park, Pennsylvania 16802, United States, [§]Department of Chemistry, Northwestern University, 2145 Sheridan Road, Evanston, Illinois 60208-3113, United States, [∥]MER Corporation, 7960 South Kolb Road, Tucson, Arizona 85706, United States, [⊥]Northwestern University/DND-CAT, Advanced Photon Source, Argonne National Laboratory, Argonne, Illinois 60439-4857, United States, and [#]Department of Materials Science and Engineering, Northwestern University, 2220 Campus Drive, Evanston, Illinois 60208-0893, United States

ABSTRACT Studies of carbon nanotube (CNT) based composites have been unable to translate the extraordinary load-bearing capabilities of individual CNTs to macroscale composites such as yarns. A key challenge lies in the lack of understanding of how properties of filaments and interfaces across yarn hierarchical levels govern the properties of macroscale yarns. To provide insight required to enable the development of superior CNT yarns, we investigate the fabrication–structure–mechanical property relationships among CNT yarns prepared by different techniques and employ a Monte Carlo based model to predict upper bounds on their mechanical properties. We study the correlations between different levels of alignment and porosity and yarn strengths up to 2.4 GPa. The uniqueness of this experimentally informed modeling approach is the model's ability to predict when filament rupture or interface sliding dominates yarn failure based on constituent mechanical properties and structural organization observed experimentally. By capturing this transition and predicting the yarn strengths that could be obtained under ideal fabrication conditions, the model provides critical insights to guide future efforts to improve the mechanical performance of CNT yarn systems. This multifaceted study provides a new perspective on CNT yarn design that can serve as a foundation for the development of future composites that effectively exploit the superior mechanical performance of CNTs.

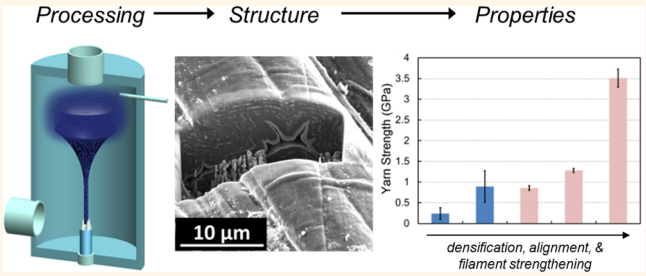

KEYWORDS: carbon nanotube · yarn · processing-structure-property relationships · multiscale Monte Carlo modeling · hierarchical composites design

Despite extensive efforts throughout the past decade to scale up the superior nanoscale mechanical properties of carbon nanotubes (CNTs) to macroscopic yarns or fibers, the promise of extending these properties to macroscopic materials remains elusive, as the strength achieved by macroscale yarns remains orders of magnitude below strengths that have been experimentally measured for individual CNTs.[1,2] To date, the highest strength and stiffness reported for CNT yarns are 8.8 and 357 GPa, respectively, for a yarn spun directly from a CNT aerogel made by chemical vapor deposition (CVD) technique and a gauge length of 1 mm.[3] Other researchers have measured maximum strengths in the range of 1–2.5 GPa for yarns spun directly from CVD aerogel,[3−5] liquid solutions,[6−8] aligned vertical arrays of CNTs,[9−17] and from twisted or rolled CNT films or mats.[18,19] These values are in stark contrast to the strength and stiffness of individual nanotubes: 100 GPa and 1 TPa, respectively.[2,20−22]

To develop a fundamental understanding of the key limitations in scaling up the strength of the nanomaterials to the macroscale, we examine the fabrication–structure–mechanical property relationships in CNT yarns made through three distinct fabrication approaches. "Directly spun" yarns were fabricated by extracting the aerogel from a CVD reactor while the CNTs were being produced, which was expected to result in

* Address correspondence to espinosa@northwestern.edu.

Received for review August 14, 2014 and accepted October 22, 2014.

Published online October 22, 2014
10.1021/nn5045504

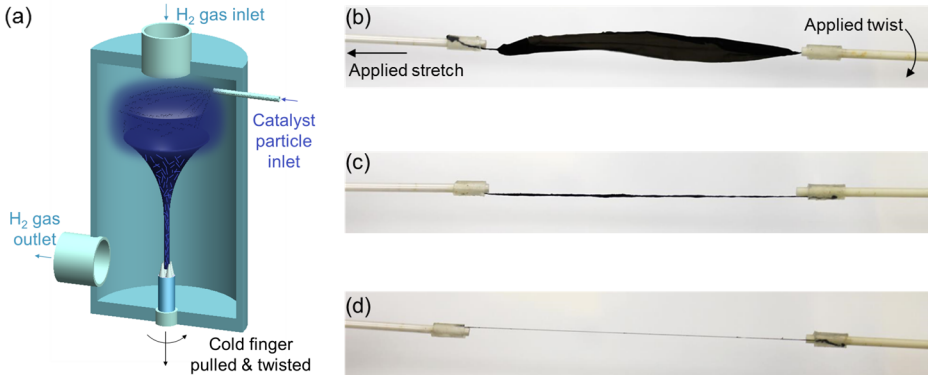

Figure 1. Schematics of processing techniques. (a) In the fabrication of directly spun yarns, catalyst particles form an aerogel of CNT bundles that is pulled and twisted by a cold finger. (b–d) In the fabrication of slowly/quickly spun yarns from mats, a ribbon of CNT bundles is stretched and rotated by independent actuators until a yarn is formed. Slowly and quickly spun yarns correspond to different rates of stretching and twisting.

well-aligned CNTs. "Quickly spun" and "slowly spun" yarns were fabricated from ribbons cut from disordered mats of CNTs. The mats were twisted and stretched in a matter of minutes for quickly spun yarns and over a period of hours for slowly spun yarns, with the expectation that the slower processing will provide sufficient time for the CNTs to untangle and align upon stretching while also resulting in less porous yarns.

We quantified the mechanical properties as a function of fabrication method by performing tensile tests. To understand the structure of the yarns, we performed scanning electron microscope (SEM) imaging of the surfaces, focused ion beam (FIB) milling into the yarn to visualize the internal structure, and wide angle X-ray diffraction (WAXD) to quantify the degree of preferred orientation in the yarns. We also developed a computational model to isolate and study the various effects of bundle strength, interface shear strength, and porosity on the overall strength of the yarns.

YARN FABRICATION

All yarns were composed of bundles of double walled carbon nanotubes (DWCNTs) prepared by MER Corporation using a CVD reactor. As described in ref 19 and subsequently in ref 23 during their production in a CVD reactor, CNT bundles are coated with a thin polymer layer similar to PMMA, referred to herein as the "inherent polymer coating". CNT bundles were fabricated into macroscopic yarns with diameters of tens of microns. The bundles in each yarn type were approximately 10–30 nm in diameter; the bundles in directly spun yarns were ~7 μm long, while those in the yarns spun from mats were ~60 μm long (see the Supporting Information). The composition of all yarns used in this study was obtained by thermogravimetric analysis (TGA).

The yarns we refer to as "directly spun" were fabricated from the CVD reactor as the CNTs were being produced. A hollow cylindrical shaped aerogel sock consisting of loosely connected CNTs was formed in the hot zone of the vertical CVD reactor and carried downstream by the flow of gas (Figure 1a). A "cold finger" spindle was inserted through the vacuum port in the lower flange of the reactor tube to contact the sock, which was stretched and twisted into a yarn by driving the spindle downward while rotating it. Following removal from the reactor, directly spun yarns were stretched and twisted to further compact the yarns. Typical stretching and twisting rates were 0.08 mm/min and 3 turns/min, respectively.

Both slowly spun and quickly spun yarns were prepared from porous CNT mats, approximately 25 cm × 25 cm in area and with an apparent thickness of 50 μm. Strips of constant width were cut from the mat, with one end of the strip then connected to a linear actuator to stretch the mat and the other end to a rotating actuator to twist the mat into a yarn (Figure 1b–d). The slowly spun yarns were stretched at a rate of ~0.1 mm/min and twisted at a rate of ~0.5 turns/min, while the quickly spun yarns were stretched at a rate of ~1.2 mm/min and twisted at a rate of ~60 turns/min. Thus, the slowly spun yarns were fabricated over a period of a few hours, while the quickly spun yarns were fabricated over a period of ~5 min. This variation in fabrication rates leads to differences in alignment and compaction of the yarns.

During postsynthesis stretching and twisting of each yarn type, a solvent was applied to the yarn to aid its compaction. The fabrication of quickly spun yarns followed the protocols established by previous publications by the authors and co-workers.[19,24] Average yarn diameters for directly spun, quickly spun, and slowly spun yarns were measured to be 49, 74, and 32 μm, respectively, based on SEM images.

STRUCTURAL CHARACTERIZATION

SEM images of the yarns reveal the organization of the CNT bundles on the surface of the yarns and qualitatively provide insight into whether the bundles are well-aligned with the yarn's axis or randomly oriented. However, visualization of the surface cannot

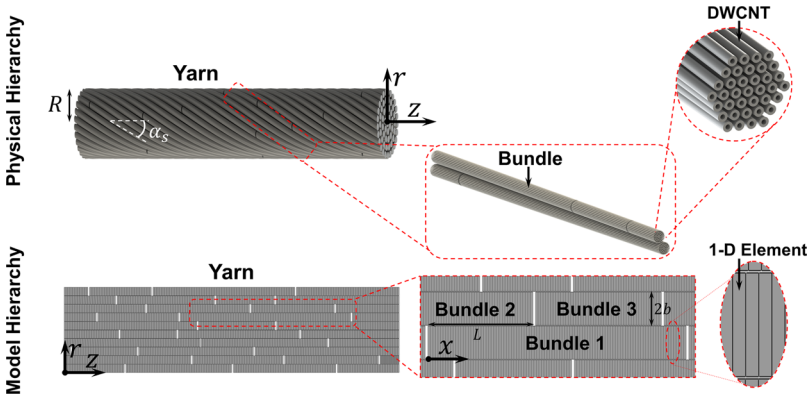

Figure 2. Schematics of idealized yarns: hierarchical structure of the 3-D idealized DWCNT yarns (top); hierarchy of CNT yarns in the Monte Carlo model (bottom). From left to right: the cross-sectional view of the yarn model, randomly distributed bundles, and a bundle discretized by 1-D elements.

provide information on the organization of the CNTs inside the yarns. To gain insight into the nature of the internal porosity of the yarns, we used a FIB (FEI Helios Nanolab Model) to mill wells into the yarns. Finally, we used wide angle X-ray diffraction (WAXD) to quantify the degree of CNT alignment through the entire cross-section of the yarns.

MECHANICAL TESTING

To quantify the tensile mechanical properties of the yarns, quasi-static tensile tests were performed. To convert the force measured to stress, the effective cross-sectional area is defined as that of the CNTs only. This area was calculated for each yarn after mechanical testing by measuring the mass, m (Mettler-Toledo microscale), and length, l, of the sample and calculating the linear mass density, $\lambda_{yarn} = m/l$. The effective area was calculated by dividing the linear density by the assumed linear density of hexagonally close packed CNTs (1.575 g cm^{-3}) and taking into account the weight contributions from a polymeric coating on the CNT bundles, remaining iron particles, and amorphous carbon using the method described in ref 24.

MODELING

To gain insight into the strength of CNT yarns in this study (denoted as "NU yarns"), we developed a stochastic Monte Carlo model to simulate the yarn fracture process. As shown in Figure 2, each yarn is assumed to consist of parallel hexagonally packed DWCNT bundles, which are analogous to "filaments" of textile-based yarns.[25] The proposed model is an idealization, aimed at incorporating insight gained from multiscale experiments to explore the upper bounds of CNT yarn properties, and it thus neglects bundle waviness (nonuniform bundle−bundle contact separation), entanglements, voids, and misalignments that exist in physical yarns.

Each bundle is discretized into a series of 1D elements. The length of 1D elements is 20 nm, much less than the overlap length (approximately 400 nm) at which the shear load transferred between two parallel bundles starts to saturate, to ensure the modeling results is mesh independent.[26] The axial position of each bundle is randomly placed to account for a random distribution of overlaps. A random strength value is assigned to each element to simulate bundle rupture. The strength values are chosen from a probability distribution that ensures that the bundle rupture strengths follow Weibull statistics

$$P(\sigma) = 1 - \exp\left[-\frac{\bar{L}}{L_0}\left(\frac{\sigma}{\sigma_0}\right)^m\right] \quad (1)$$

where σ is the applied stress, σ_0 is a scale factor, m is the shape parameter, $\bar{L}$ is the bundle length, L_0 is a reference bundle length, and $P(\sigma)$is the failure probability of the bundle under stress σ.

The stress distribution within the yarn is approximated by a simplified load-sharing rule. After applying a load to the yarn, stress is redistributed so that the stress in each element does not exceed the threshold value the element can take. The threshold is the minimum of two values—the assigned strength of the element and the upper bound of the tensile stress that can be transferred through the shear interaction between its neighbors (explained later). The former determines when the bundle rupture happens; the latter determines when interbundle sliding occurs. The load lost at the location of a broken bundle is transferred to its nearest neighbor bundles to satisfy force equilibrium at each cross section of the yarn. Compared with previous Monte Carlo models,[27,28] the current model has two improvements: (1) we implemented an algorithm to discriminate "effective" and "ineffective" contacts between two adjacent filaments (in NU yarns, DWCNT bundles), and (2) we incorporated the inherent shear strength and stiffness between bundles found through experiments,[26] while previous models used the classic friction law, which requires non-zero twist for any load transfer between bundles to occur. The algorithm to evaluate the effectiveness of

contact between two adjacent bundles is based on the relative positions of the two bundles. If the bundle under consideration is shorter than the adjacent bundle, and both ends of the bundle are completely enclosed by the adjacent bundle, the contact is defined as "ineffective", and we assume there is no load transfer through this contact (*e.g.*, contact between bundle 1 and bundle 3 in Figure 2). If only one end of a bundle lies between the two ends of the adjacent bundle, the contact is defined as "effective" (*e.g.*, contact between bundle 1 and bundle 2 in Figure 2), meaning that load can be transferred between the two adjacent bundles through their interface. The elastic solution for the shear-lag model introduced in ref 29 was used to calculate the stress distribution, $\sigma(x)$, in each bundle along the overlap region for an "effective" contact, namely

$$\sigma(x) = \frac{2\tau_f}{b\lambda}\frac{1}{\cosh\left(\frac{\lambda L}{2}\right)}\sinh\left(\frac{\lambda x}{2}\right)\cosh\left(\frac{\lambda(L-x)}{2}\right) \quad (2)$$

where $\lambda = (2G/(Ebh))^{1/2}$, E is the bundle elastic modulus, $2b$ is the equivalent bundle thickness, G is the shear modulus of the bundle−bundle interface, h is the thickness of the interface, x is the distance to the free end of the bundle, L is the overlap length, and τ_f is the interfacial shear strength. For the CNT yarns studied here, b and h are approximately 6.1 and 2.5 nm, respectively.[26] Equation 2 gives the maximum tensile stress that the shear load transfer can introduce to the element at location x.

As increasing load is applied, bundle rupture occurs if the axial stress in any element of a bundle reaches its assigned strength. When this occurs, the failed element is deactivated (its stress is set to zero), and new sub-bundles and contact pairs are generated on either side of the rupture. The model determines whether the new contacts are "effective" or "ineffective," and then it redistributes the axial load to the unbroken bundles until force balance is satisfied. During simulations, the model ensures force equilibrium, but the bundle deformation and bundle−bundle sliding are not computed. Thus, the model output contains the yarn stress, but not yarn strain. The yarn is deemed as having failed when no additional load can be supported by the remaining load carrying bundles.

In the current model, yarn twisting is taken into account by applying a radial distribution of the bundle stress in the yarn. For an ideal helical twisted yarn with a surface twist angle, α_s, the bundle axial strain $\varepsilon_b(r)$ at radial position r is given in ref 25 as

$$\varepsilon_b(r) = \varepsilon_y(\cos^2\alpha_r - v_T\sin^2\alpha_r) \text{ where}$$
$$\alpha_r = \tan^{-1}(r/r_0\tan\alpha_s) \quad (3)$$

In eq 3, r_0 is the yarn radius, $\alpha_r$is the twist angle of the bundle at radial position r, $\varepsilon_y$is the macroscopic yarn strain, and $v_T \sim 0.8$ is the Poisson's ratio of the yarn.[19] The bundle stress variation along the yarn radial direction is set using eq 3 and the bundle elastic modulus, E.

Yarn microporosity is also taken into account in the model because non-zero porosity reduces the effective interactions between overlapping bundles. Since load is transferred between adjacent bundles through shear forces, reducing the density of nearest neighbor bundles leads to a reduction in the load-bearing capacity of the material. We model distributed microporosity by decreasing the maximum shear stress between bundles by a multiplication factor of $(1 - p)$ for a yarn with porosity p.

Filament rupture and interface sliding are the two main competing failure mechanisms for composites containing hierarchical architectures.[29−34] Therefore, having an accurate description of the properties of both filaments and interfaces is essential for the model's predictive capabilities. For the NU yarns investigated here, the properties of the bundles and the bundle−bundle interfaces were characterized through nanoscale experiments and computations. Weibull analysis on the bundle rupture strength for individual as-received or "pristine" DWCNT bundles (30 nm in diameter and 5 μm long) yields a scale factor σ_0 = 2.8 GPa (63% failure probability) and a shape factor $m = 2.2$.[35] Fitting the results from *in situ* SEM shear tests on pairs of parallel bundles using the shear lag model reveals an effective interface shear modulus of 10 MPa and shear strength of 350 MPa.[26,29]

To demonstrate the model's predictive capabilities, we also modeled the CNT yarns prepared using the "wet-spinning" method at Rice University,[36] here termed "Rice yarns". In the Rice yarns, the "filaments" are individual MWCNTs with an average length of 5 μm and an average diameter of 3.2 nm. The mechanical properties of these MWCNTs (*i.e.*, the filaments of the Rice yarns) have not been studied experimentally and have to be approximated from independent studies. Tensile tests on MWCNTs performed by Yu *et al.*[37] yield a scale factor of 31.5 GPa (note the stress in ref 37 was defined by assuming only the outer shell of a MWCNT bears the load) and a shape parameter of 2.4. Converting the stress value to a nominal stress by accounting for the cross-sectional area of all of the shells, the scale factor for the MWCNTs in Rice yarns, with mostly triple-walled CNTs, is approximated as 14.8 GPa, and the shape parameter remains the same. Based on experiments performed to measure the shear interface properties between two parallel MWCNTs, the interfaces between CNTs in the Rice yarns are assumed to have a shear strength of 60 MPa and a shear stiffness of 100 MPa.[29] The geometrical and mechanical properties of the filaments and interfaces for NU and Rice yarns are summarized in Table 1.

TABLE 1. Geometrical and Mechanical Properties of Yarn Filaments and Interfaces in NU and Rice Yarns

	parameters	NU yarns	rice yarns
simulation inputs	filament	DWCNT bundles	MWCNTs
	filament diameter (nm)	~10−30	~2−5
	filament length, L (μm)	60	5
	filament elastic modulus, E (GPa)	60	400
	Weibull scale factor, σ_0 (GPa)	2.8	14.8
	Weibull shape factor, m	2.2	2.4
	interface shear modulus, G (MPa)	10	100
	interface shear strength, T_f (MPa)	350	60
	surface twisting angle, α_s (deg)	~15	~0
	porosity, p	~60	~0
model prediction vs experiments	experimental yarn strength (GPa)	0.95 ± 0.40	1.0 ± 0.2
	predicted yarn strength (GPa)	0.84 ± 0.04	1.2 ± 0.07

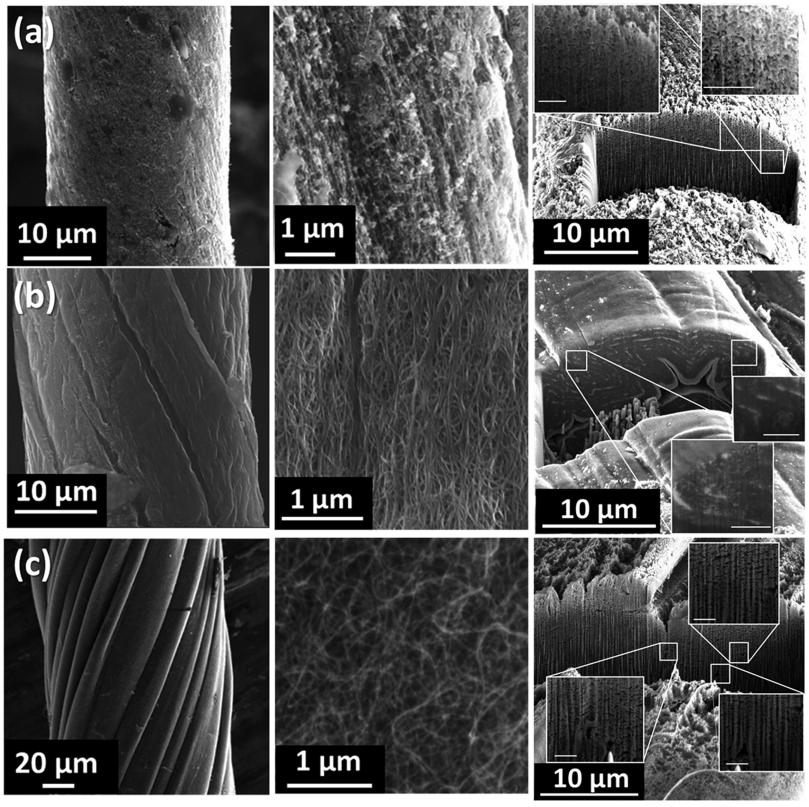

Figure 3. Structural characterization. SEM images of (a) directly spun, (b) slowly spun, and (c) quickly spun yarns, where the first column shows the yarn morphology, the second shows the arrangement of CNT bundles on the surface of the yarn, and the third shows wells machined into the yarns using FIB to reveal the internal porosity and morphology of the yarns. Inset scale bars are 1 μm.

RESULTS AND DISCUSSION

Structural Characterization. Inspection of the surfaces of the three types of yarns through SEM imaging (Figure 3) reveals contrasting CNT orientations. Quickly spun yarns have a random distribution of orientations of the CNTs on the surface of the yarns, where the organization of CNTs still resembles the original disorganized mat structure. This is expected since these yarns were made quickly by twisting and moderately stretching ribbons of the mat, introducing an effective tensile strain of only about 6% toward untangling and orienting the CNTs with the yarn's tensile axis. The directly spun yarns have the highest degree of CNT alignment on the surface of the yarns. Since these yarns were fabricated by pulling the CNTs out of the CVD reactor while they are made, it is expected that this fabrication technique should result in a high degree of alignment. However, wavy strands of CNT bundles are present on the surface of all yarns. The slowly spun yarns have an intermediate degree of CNT alignment on their surfaces. It is expected that the alignment of CNTs in these yarns, fabricated from the same disordered mats of CNTs as the quickly spun

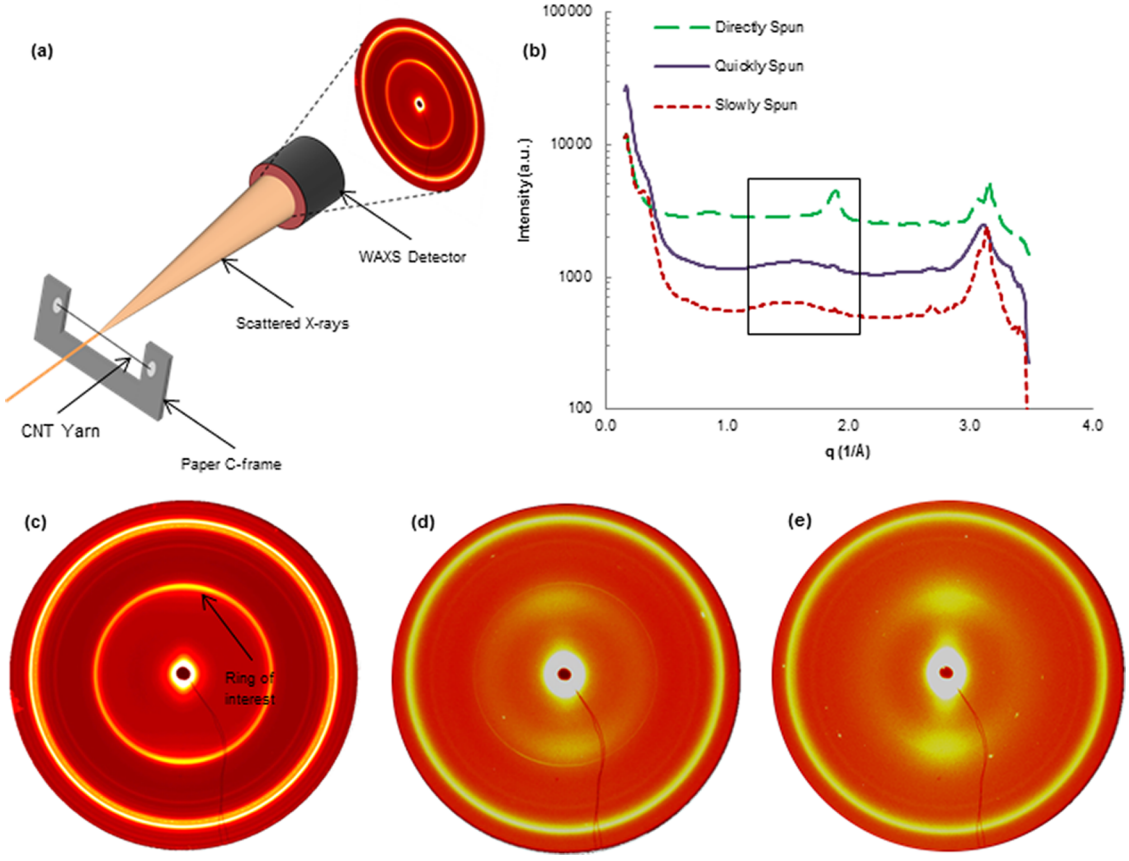

Figure 4. WAXD analysis. (a) Schematic of setup for WAXD analysis of CNT yarns. (b) Intensity versus scattering vector from WAXD patterns for the three different yarns (CNT diffraction peak at q = 1.89/Å is within the boxed region). Representative 2D WAXD scattering patterns of (c) directly, (d) quickly, and (e) slowly spun yarns.

yarns, should be higher than that of the quickly spun yarns since a larger axial strain is introduced (~12%) over the much slower, and therefore longer, processing time, which gives time for the network of CNTs to relax as tension is applied.

The overall porosity, p, of the yarns can be calculated using the following equation

$$p = 1 - \left(\frac{D_{\text{effective}}}{D_{\text{outer}}}\right)^2 \quad (4)$$

where $D_{\text{effective}}$ corresponds to the diameter from linear density assuming a "filled" circular cross section and D_{outer} is the outer diameter of the yarn as measured in the SEM. The average porosities of representative directly, quickly, and slowly spun yarns was found to be ~77%, ~72%, and ~55%, respectively.

To determine the nature of the porosity, FIB was performed to visualize the internal structure of each type of yarn. The FIB studies reveal that the directly spun yarns have a large amount of microporosity, defined here as having pores with characteristic dimensions of less than 0.2 μm, distributed throughout the diameter of the yarns. The slowly spun yarns are very compact, and have a very small amount of microporosity, but have large voids (defined as having characteristic dimensions of 1 μm or more) present where the folds of the initial ribbon of mat have not fully come into contact. The quickly spun yarns have both large pores present and a large amount of microporosity.

Pores do not affect the definition of the cross sectional area, since they are removed by weighing the sample to calculate the effective area; however, these porous regions may adversely affect the mechanical properties of the CNT yarns. While the voids are expected to close during tensile deformation due to the helical yarn providing radial compression with axial tension, these porous regions may consist of wavy, misaligned CNTs that do not effectively contribute to supporting the axial load, or other local defects through which the tensile stress is not effectively transferred between bundles surrounding voids. Thus, it was expected that there would be a trade-off between the good alignment and the high porosity of the directly spun yarns. The slowly spun yarns should, therefore, have the best mechanical properties due to increased alignment over the quickly spun yarns, and greatly decreased porosity over the directly and quickly spun yarns.

Wide angle X-ray diffraction provides information about the alignment of the CNTs within the yarns

through the entire cross section of each yarn. The 2D WAXD scattering patterns of the CNT yarns and their respective 1D data, obtained by summing the intensities along the azimuthal scan and plotted as a function of scattering vector q, are shown in Figure 4. The diffraction peak at a scattering vector of q = 1.89 /Å, corresponding to the DWCNT internal wall spacing (d = 3.32 Å), is pronounced for the directly spun yarns, but in the cases of the quickly and the slowly spun yarns, the peaks at this scattering vector are much less pronounced (Figure 4b). Instead there are broad, diffuse peaks around q = 1.54 /Å, which could correspond to the spacing between adjacent CNTs within a bundle (d = 4.08 Å). Thus, for directly spun yarns in which the diffraction peak is concentrated at q = 1.89/Å, we believe that the CNTs in the bundles are in close contact with each other throughout the bundle and that their inter CNT distance is similar to the DWCNT interlayer spacing. Conversely, in the bundles of the slowly and quickly spun yarns, the CNTs may be convoluted inside the bundle, meaning that they are not in close contact along the length of the bundles, and thus their inter CNT spacing varies throughout the bundle, producing a diffuse and shifted peak at q = 1.54 /Å. For a more detailed analysis please see Supporting Information.

Azimuthal integrated scans of the intensity of the 2θ = 9.98° ring, corresponding to the spacing of the two walls comprising each DWCNT within the bundles, were obtained from each 2D image. To quantify the degree of preferred orientation of the CNTs within the yarns, we calculate the Herman orientation factor (HOF) for each yarn using the following equations

$$f_H = \frac{3\langle \cos^2 \phi \rangle - 1}{2} \quad (5)$$

$$\langle \cos^2 \phi \rangle = \frac{\int_0^{\pi/2} I(\phi) \cos^2 \phi \sin \phi \, d\phi}{\int_0^{\pi/2} I(\phi) \sin \phi \, d\phi} \quad (6)$$

where ø is the angle between the axis of interest (CNT axis) and the reference direction (the yarn axis).[38,39] For a perfectly aligned sample, the HOF would be 1 and for a yarn where the CNTs are randomly oriented and the HOF would be 0.

For each yarn, WAXD patterns were obtained for three to four points along the length of the yarn. The incident X-ray beam conditions were kept constant for all data points, but the exposure times were varied for each type of yarn (100 s for directly spun, 15 s for quickly spun, and 4 s for slowly spun yarns) to account for the disparate masses of each yarn type. The average values of the HOF across these points were calculated for each yarn and are tabulated in Table 2. The directly spun samples have low HOF values (average HOF = 0.049) compared to the slowly spun (average HOF = 0.346) and quickly spun samples (average HOF 0.338). We note that, as discussed previously, through FIB and SEM visual inspection, as well as analysis of the tensile stress–strain behavior of these directly spun yarns (see below), which is relatively linear until failure, it would appear that the directly spun samples have well-aligned CNTs.

TABLE 2. Summary of WAXD Results and Mechanical Properties by Yarn Type[a]

		experimental yarn type		
	parameters	directly	quickly	slowly
WAXD results	HOF_{avg}	0.325 (0.049*)	0.338	0.346
	HOF_{max}	0.464 (0.072*)	0.390	0.368
	HOF_{min}	0.193 (0.014*)	0.306	0.324
mechanical properties	E_{avg} (GPa)	12.1 ± 7.3	27.3 ± 10.9	79.4 ± 44.0
	E_{max} (GPa)	24.8	42.7	208.3
	σ_{avg} (GPa)	0.24 ± 0.15	0.55 ± 0.11	0.95 ± 0.40
	σ_{max} (GPa)	0.626	0.773	2.375
	ETF_{avg} (J-g^{-1})	5.3 ± 2.9	40.1 ± 25.3	18.4 ± 15.3
	ETF_{max} (J-g^{-1})	9.8	89.6	71.4

[a] Note that the HOF values with an asterisk correspond to values with waviness.

We hypothesize that since the directly spun samples are more porous than the slowly and quickly spun samples, the waviness of the CNTs within the samples affect the WAXD results of the directly spun sample significantly. We note that the linear densities of directly spun yarns (~0.7 μg/mm) are about 3–5 times lower than the quickly (~1.9 μg/mm) or slowly spun yarns (~3.4 μg/mm); thus, if a small amount (*e.g.*, 0.1 μg/mm) of wavy CNTs is incorporated into or on the directly, quickly, and slowly spun yarns, that amount will more heavily influence the data for the directly spun yarns.

In order to evaluate and remove the effect of waviness from the WAXD analysis of directly spun samples, a second set of analyses were performed in which the intensities were first integrated over the azimuthal ring, and then the background, taken as the baseline intensity over the entire 2θ = 9.98° ring, was subtracted (Figure S4, Supporting Information). Once the effect of waviness is removed with this approach, the HOFs increase significantly (to an average HOF of 0.325 for directly spun yarns), correlating with the previously drawn conclusions from SEM imaging and mechanical testing.

Thus, we hypothesize that at least the shell of the directly spun yarns contains well-aligned CNTs, whereas the porous core may contain some misaligned CNTs that do not directly support the tensile load.

Mechanical Testing. Stress–strain curves are presented in Figure 5a for representative samples of each of the three types of yarns. For each yarn, the modulus was calculated as the initial slope of the stress–strain curve, the strength was calculated as the maximum stress value, and the energy to failure was calculated as the area under the force-strain curve, normalized by

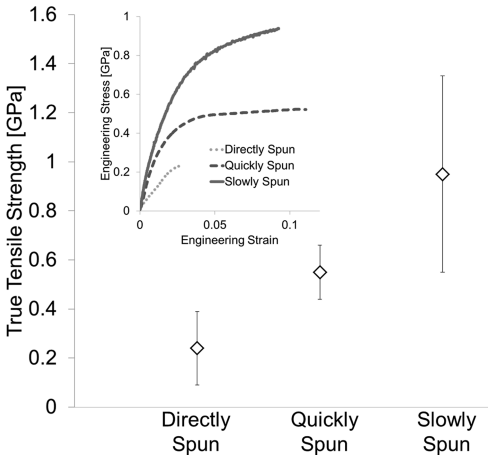

Figure 5. Mechanical characterization. True tensile strength values for different yarn types. Averages shown as white diamonds, with error bars of ±1 standard deviation. Inset: engineering stress–strain curves for representative yarns by type.

the linear mass density of the yarn. Modulus and energy to failure are reported in terms of engineering values using the initial cross section of the DWNTs within the yarn, while true strength values are reported in terms of the cross section of the DWNTs in the yarn before failure.

As shown in Figure 5a, the stress versus strain behavior for the directly spun yarns was approximately linear to failure. The strain to failure in directly spun yarns was always less than 11%, compared to maximum strains of 27% for quickly spun, and 22% for slowly spun yarns. This supports the previous assertions that the directly spun yarns contain at least a shell of well-aligned CNTs that support the load until failure. The stress–strain curves for the slowly and quickly spun yarns exhibit an initial linear regime followed by a nonlinear response in which the strength continues to increase with strain. For the quickly spun yarn, the slope of the nonlinear regime is low. This large deformation response corresponds to a major rearrangement of the network of misaligned CNTs, which results in much higher failure strains than for the directly spun yarns, in which the aligned CNTs at the surface carries the load until abrupt failure without large CNT network rearrangement. The slowly spun yarns presented, in general, a much stiffer behavior in the nonlinear regime, which is consistent with a denser, more aligned CNT structure leading to a more brittle behavior when compared to the quickly spun yarns.

The mechanical properties are summarized in Table 2. The average strengths of the directly, quickly, and slowly spun yarns were found to be 0.24, 0.55, and 0.95 GPa, respectively. The average modulus values of the directly, quickly, and slowly spun yarns were found to be 12.1, 27.3, and 79.4 GPa, respectively. Thus, in terms of strength and modulus, the better surface alignment of the directly spun yarns was outweighed by the high porosity and possible internal misalignment. Any misaligned or ineffective CNTs add weight without adding strength to the yarn. The slowly spun yarns had the highest strengths, as they had increased alignment over the quickly spun yarns and they were significantly more compact than the other two types of yarns. We also note that the CNT bundles in the directly spun yarn are ~7 μm long, compared to the ~60 μm in the slowly and quickly spun yarns, which has been shown to be an important parameter in yarn properties, with longer CNTs resulting in higher properties.[8,40] Regarding the energy to failure (ETF), a measure typically associated with material toughness, we found that the slowly and quickly spun from mats yarns achieved higher values (18.4 J-g^{-1}, and 40.1 J-g^{-1}, respectively) than the directly spun yarns (5.3 J-g^{-1}) for the reasons previously discussed.

Modeling Results. Using the Monte Carlo model, NU yarn model structures with a diameter of 285 nm and a length of 240 μm, as well as Rice yarn models with a diameter of 35 nm and a length of 20 μm were simulated. At the start of the simulations, each NU yarn consists of 340 bundles with a diameter of 25 nm and an average length of 60 μm; each Rice yarn consists of 340 triple-walled CNTs with an outer diameter of 3.2 nm and an average tube length of 5 μm. For each system, 100 Monte Carlo simulations were performed, and the average and standard deviation of the yarn strength were calculated from these results. First, simulations were performed on both yarns with ideal helical twisted geometries (*i.e.*, filaments were perfectly aligned and there was no porosity in yarns). In this way, the model predicts an upper bound of average yarn strength by neglecting the complexity from material preparation.

For the ideal NU yarns, the predicted yarn strength was 1.45 ± 0.07 GPa; for Rice yarns, the predicted yarn strength was 1.2 ± 0.07 GPa. Even though the predicted strength values for both yarns were similar, the model predicts different dominant failure mechanisms. Figure 6a gives the simulated numbers of filament ruptures in two yarns during tensile tests. For the ideal NU yarn, the first bundle rupture occurred very early, at a small applied stress of 0.2 GPa, and the rupture rate accelerates gradually until the yarn fails. This suggests that in the idealized NU yarns, the bundle strength is the bottleneck that limits the yarn performance. In contrast, MWCNT rupture in Rice yarn occurred much later, at a large applied stress of 1.0 GPa, and the total number of ruptured tubes only reached 12 when yarn failure occurred due to tube sliding and pull-out. This suggests that the interface strength is the bottleneck that limits the Rice yarns' performance (Table 1).

X-ray and electron microscopy studies on Rice yarns showed 5 μm long MWCNTs aligned nearly perfectly (some bundle waviness is observed in SEM images)

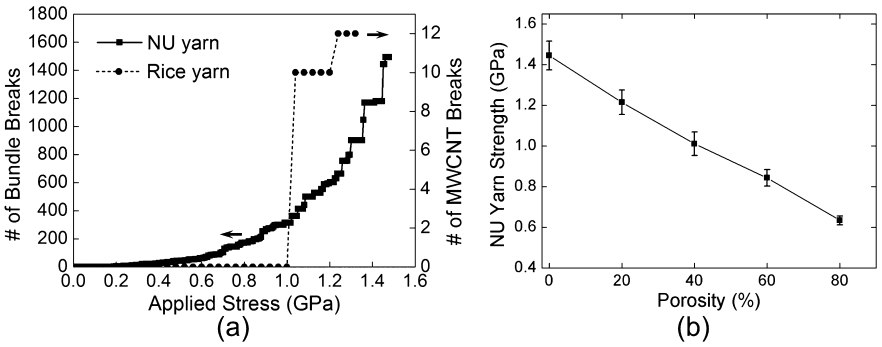

Figure 6. Model predictions of current yarns. (a) Number of ruptured filaments as a function of applied axial stress as predicted by the Monte Carlo model for NU and Rice yarns. (b) Predicted decrease in yarn strength due to porosity (NU yarns).

along the axial direction, with no appreciable yarn porosity. Therefore, the actual microstructure in the Rice yarns is very close to the idealized yarn structure assumption presented here. However, the NU yarns have complicated microstructures that feature bundle misalignment, waviness, and entanglement, as well as non-negligible yarn porosity. In addition, at locations where the PMMA-like inherent polymer coating on the bundle surface is thicker than the thin interface containing only 4- to 8- mer chains that was characterized in ref 26, the polymer shear strength could drop from 350 MPa and approach 30−70 MPa for bulk material.[41] All of these features may lower the effective interface shear strength.

FIB and SEM characterizations indicate that the porosity in NU yarns ranges from 50% to 80%. Figure 6b shows that the predicted yarn strength drops almost linearly with yarn porosity up to 80%. As the porosity increases, individual bundles have a fewer number of contact bundles. Thus, the dominant failure mechanism becomes interface sliding. For example, the final number of bundle ruptures for 60% porous NU yarns is only 382 at an ultimate stress of 0.84 GPa compared with 1494 for the ideal helical NU yarns at an ultimate stress of 1.45 GPa; thus, more porous yarns result in less effectively accessing the full bundle strengths within the yarns.

The model predicted yarn strength is compared with the experimental measurement in Table 1. The predicted yarn strength for a 60% porous yarn of 0.84 ± 0.04 GPa agrees very well with the experimental measurements for slowly spun yarns (0.95 ± 0.40 GPa), however, the model does not capture the measured standard deviation of strength values for these yarns. This is to be expected for this simplified model, which does not include the effect of bundle misalignment.

DISCUSSION

The purpose of the present study is to develop fundamental understanding for the processing-structure-property relationships in CNT yarns through experimental, analytical, and computational modeling efforts. The key factors that we have identified that can contribute to variations in CNT yarn strength include: bundle strength (which is a function of bundle diameter), bundle length, interfacial strength, CNT alignment within yarns, and porosity.

Modeling of Rice yarns suggests that the weak tube−tube interface is limiting the mechanical strength of yarns made of highly aligned, but relatively short, CNTs. Therefore, increasing the interface strength would be an effective way of improving the tensile strength of Rice yarns (Figure 7a). The model suggests that the yarn strength increases by a factor of about 7 when the interface shear strength increases from 60 to 700 MPa. Note in the modeling the range of the interface shear strength was chosen to demonstrate the effect of interface shear strength on yarns' mechanical properties and the transition between two dominant failure mechanisms. It is not meant to model a specific interface material. As the interface becomes stronger, the dominant failure mechanism will transition from interface sliding to tube rupture, and the ultimate yarn strength will saturate at about 7 GPa. Recent density functional theory calculations suggest that defects improve CNT−CNT shear interactions at the expense of CNT tensile strength.[42] In this context, it is worth revisiting the CNT yarns synthesized by Koziol *et al.*, one of which was reported to have the highest strength of 8.8 GPa.[3] Those yarns contain mainly double-walled CNTs of large diameter (4−10 nm), and Koziol *et al.* pointed out that the shells of these double-walled CNTs collapsed against each other into a "dog-bone" cross-section. Consequently, the contact area between adjacent tubes was greatly enhanced. This is equivalent to improving the interaction between CNTs, the lack of which was the key factor limiting Rice yarns' strength. In other words, the CNT yarns synthesized by Koziol *et al.* have the fibril strength comparable to that in Rice yarns but with improved interfacial properties.

In contrast, for the microstructures observed in NU yarns, yarn strength can be improved with various strategies at different stages of fabrication. For the present NU yarns, the weak effective bundle−bundle interface strength due to bundle misalignment and

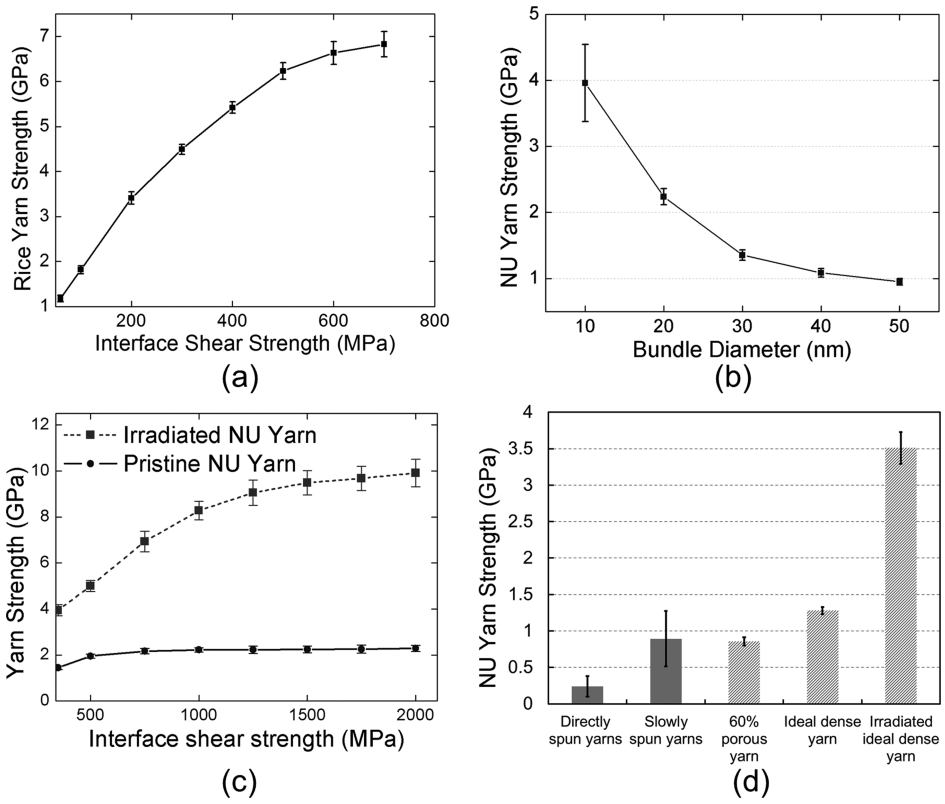

Figure 7. Model predictions for yarn improvements. (a) Predicted yarn strength improvement due to tube−tube interface strengthening for Rice yarns. (b) Predicted yarn strength as a function of bundle diameter for NU yarns. (c) Model prediction of the effect of interface shear strength on the strength of pristine (blue circles) and irradiated (red squares) NU yarns. (d) Comparison of experimental results (solid columns) with model predictions (dashed columns) showing the effects of various strategies to improve NU yarn strength.

large yarn porosity greatly limits the yarn strength. Therefore, methods for both improving bundle alignment and increasing densification of the yarns must be identified. However, once the ideal helical twisted yarns are made, bundle rupture may become the dominant failure mechanism that limits the yarn strength; thus, methods for increasing the bundle strength must also be identified.

Two approaches that could be used to increase bundle strength are to decrease the bundle diameter, or to cross-link tubes within bundles. As noted by Filleter *et al.*,[35] the effective strength of DWCNT bundles is much lower than the strength of individual DWCNTs because bundles bear load mainly through the tubes in the outer layer. Therefore, reducing the bundle diameter will increase the ratio of the number of external to internal tubes and thus increase the *effective* bundle strength. Figure 7b predicts that the average yarn strength could reach 2.1 GPa if the bundle diameter were reduced to 10 nm. This could be implemented with modified manufacturing approaches.

Another approach toward improving bundle strength is to introduce cross-links between CNTs inside the bundle through chemical treatments or irradiation. Electron beam irradiation performed on individual bundles of CNTs inside a transmission electron microscope (TEM) can improve the load transfer between tubes inside the bundle by introducing cross-linking between tubes, leading to an increase in *effective* bundle strength from 2.8 to 17.1 GPa, and an optimized increase in modulus from 60 to 550 GPa.[35] Figure 7c illustrates how the yarn strength is predicted to vary as a function of interface shear strength for pristine (nonirradiated) and irradiated yarns. In the latter, the bundle Weibull distribution is scaled to $\sigma_0 = 17$ GPa with all other parameters the same. We note that in the simulations, we increased the shear strength of the bundle−bundle interface but kept the shear modulus constant. Under these conditions, pristine yarns are predicted to benefit only moderately when the interface shear strength is increased and the maximum average yarn strength saturates at about 2.5 GPa. In contrast, irradiated yarns are predicted to reach strengths of 3.9 GPa even when the interface shear strength remains constant (350 MPa). In yarns containing heavily cross-linked bundles, the dominant failure mechanism predicted by computational modeling is expected to change from bundle rupture to interface sliding. Therefore, improving the interface shear strength has the potential to significantly increase the average yarn strength to reach values as high as 10 GPa.

We note that in the study by Filleter *et al.*,[35] individual bundles were subject to electron-beam induced

cross-linking inside a TEM. As discussed in ref 43, it is not yet possible to extend this process of irradiating bundles at the nanoscale to the macroscale yarn fabrication techniques; thus the manufacturing of yarns from irradiated bundles is not yet feasible. Moreover, irradiation of mats containing bundles coated with a polymer, as is the case for the NU yarns, another challenge emerges. Typical radiation doses needed to cross-link CNTs inside a bundle are orders of magnitude higher than those needed to cross-link polymers and would result in polymer radiation damage. This challenge calls for novel manufacturing strategies that can take full advantage of constituents and their interfaces.

The results from experiments and Monte Carlo simulations assuming pristine perfectly aligned yarns with varying levels of porosity and irradiation are summarized in Figure 7d. The similarity between the strength measurements in slowly spun yarns and the model predictions, using 60% porosity, is striking. Ideally dense yarns perform only slightly better. However, when yarns are irradiated at the optimal dose to induce cross-linking within bundles throughout the yarn, a major improvement in strength is predicted. As discussed in relation to the role of interface shear strength, Figure 7c, even much more dramatic improvements are possible through the use of tougher and stronger polymers.

CONCLUSIONS

Fabrication of macroscopic yarns from CNTs can be achieved through numerous processing techniques, resulting in a variety of yarn architectures and resulting mechanical properties. This work systematically demonstrates, through experimental characterization and computational modeling, the effect of fabrication technique on key features that limit yarn performance: porosity and CNT alignment. In addition, through computational modeling, the relative importance of interfacial strength and bundle strength is revealed, as well as upper bounds of strength that could be achieved through processing improvements. While the model neglects several detrimental structural features resulting from *current* processing conditions, it explores how yarn performance could be *further* improved if these problems could be eliminated. Therefore, the model complements the experimental analysis of the effects of porosity and misalignment on mechanical behavior by exploring how other factors (such as filament and interfacial strength) can affect yarn performance.

For substantial advances in the properties of macroscopic CNT yarn performance, the structure and properties of CNT yarns must be optimized at all of the hierarchical levels comprising these yarns: from the individual CNTs, to bundles of CNTs, to networks of CNTs, and finally the macroscopic yarn structure. Future research efforts aimed at each of the following should be pursued to improve yarn mechanical performance: (1) increasing the bundle strength through the introduction of cross-links at the bundle network level (*i.e.*, the development of a technique that can be applied to cross-link bundles in large mats of CNTs, or macroscopic CNT yarns); (2) improving the load transfer between adjacent CNTs through the identification and application of a coating on CNT bundles with increased strength and stiffness over current inherent coatings (*e.g.*, the development of techniques to functionalize CNT bundles inside the CVD reactor, or after fabrication, to provide tougher interfaces between CNTs); (3) developing fabrication methods for alignment of straight (*i.e.*, fully extended, and not wavy) CNTs and CNT bundles; and (4) identifying effective chemical or mechanical methods for compaction of yarns to reduce porosity and ensure CNTs are connected and utilized within the yarn. We believe that through the development of the above improvements, higher mechanical properties be realized, and through the production of a better defined architecture of CNTs the electrical and thermal properties of macroscopic yarns would also be enhanced.[1]

Current CNT yarns have scratched the surface of the promise of scaling up CNT properties, and with the comprehensive understanding of processing-structure-property relationships developed herein and, thus, a concerted effort on improvements of key structures through variations in fabrication processes, gains are still to be made in this field. It is reasonable to infer from our findings that the major challenge lies in the field of manufacturing. Indeed, current manufacturing methods exploiting liquid crystal precursors produce highly aligned CNT yarns but at the expense of limited control of the chemistry of interfaces and bundle length. By contrast, CVD-synthesized CNT yarns can achieve very rich chemical functionalization on the surface of CNT bundles but lack the control needed in assembling CNTs to produce ordered hierarchical structures. In this regard, inspiration from natural materials, which exhibit exquisite arrangement of constituents across multiple length scales, and development of templated self-assembly approaches seem promising.

MATERIALS AND METHODS

Solvents Used in Yarn Fabrication. As noted in the main text, each yarn was sprayed with a solvent to facilitate fabrication and compaction of the yarns. 1,2-Dichloroethane (DCE) was used on all yarn types, while DCE or sulfuric acid was used on slowly spun yarns to determine the effect of solvent type on yarn properties.

A *t* test was used to analyze whether the difference in average modulus, average strength, or average energy to failure

for the slowly spun yarns with the two different solvents was statistically significant. The results in Table S1 (Supporting Information) indicate that there is no significant difference (two-tailed p-value > 0.05) between the two sets for any of these three mechanical performance parameters, suggesting that there is no appreciable difference in the yarn performance between the use of DCE or sulfuric acid. The identification of an optimal solvent remains an important area for future research in carbon nanotube yarn development.

Wide Angle X-ray Diffraction. The WAXD studies were performed at Argonne National Laboratory's Advanced Photon Source (APS beamline 5ID-B). The synchrotron X-rays were produced with an APS standard undulator A. The beamline's double Si(111) monochromator was set for 17.4 keV (wavelength of 0.71 Å). The WAXD patterns were recorded with a MAR165 CCD X-ray detector, with a sample to detector distance of 19.2 cm and a square spot size of 250 μm defined by collimating slits. In the 2-dimensional diffraction patterns produced by the CNT yarns, a reading at $2\theta = 9.98°$ corresponds to the 002 planes of the CNTs perpendicular to their longitudinal axes, and the azimuthal spread of those reflections indicates how aligned the CNTs are with the yarn axis.

Mechanical Testing. For each test, each end of the yarn was first affixed to a paper end tab with epoxy. The tabs were clamped into a screw-driven microtesting frame (Fullam, 2000 lb test frame) and stretched in tension, while the load was recorded with a 250 g load cell (Honeywell, Model 31, resolution of 2 mg), and the elongation of the yarn was recorded using a linear variable differential transformer (Allison Model HS50, resolution of 1 μm). The gauge lengths of the yarns varied from 5 to 20 mm. Quasi-static tests were performed with strain rates on the order of 2×10^{-4} s^{-1}. Misalignment between the tensile axis of the yarn and the direction of applied displacement was less than 5° in all tests.

Conflict of Interest: The authors declare no competing financial interest.

Supporting Information Available: Additional details regarding measurement of bundle diameter, estimation of bundle length, and wide angle X-ray diffraction analysis; HR-TEM image of DWCNT bundle (Figure S1); WAXD variations of HOFs at different points within yarns (Figure S2); example 2D WAXD pattern and intensity versus distance scan (Figure S3); WAXD HOF values of directly spun samples with and without the effect of waviness (Figure S4); comparison of mechanical properties of slowly spun yarns with different solvents (Table S1). This material is available free of charge *via* the Internet at http://pubs.acs.org.

Acknowledgment. This work was supported by ARO MURI award W911NF-09-1-0541. Portions of this work were performed at the DuPont–Northwestern–Dow Collaborative Access Team (DND-CAT) located at Sector 5 of the Advanced Photon Source (APS). DND-CAT is supported by E.I. DuPont de Nemours & Co., The Dow Chemical Company, and Northwestern University. Use of the APS, an Office of Science User Facility operated for the U.S. Department of Energy (DOE) Office of Science by Argonne National Laboratory, was supported by the U.S. DOE under Contract No. DE-AC02-06CH11357. Part of this work was performed in the EPIC facility of NUANCE Center at Northwestern University. The NUANCE Center is supported by NSF-NSEC, NSF-MRSEC, the Keck Foundation, the State of Illinois, and Northwestern University. M.R.R. acknowledges support from the Department of Defense (DoD) through the National Defense Science & Engineering Graduate Fellowship (NDSEG) Program. M.R.R. and M.F. acknowledge the Northwestern University Ryan Fellowship. We thank Rafael Soler-Crespo for helpful discussions.

REFERENCES AND NOTES

1. De Volder, M. F. L.; Tawfick, S. H.; Baughman, R. H.; Hart, A. J. Carbon Nanotubes: Present and Future Commercial Applications. *Science* **2013**, *339*, 535–539.
2. Peng, B.; Locascio, M.; Zapol, P.; Li, S.; Mielke, S. K.; Schatz, G. C.; Espinosa, H. D. Measurements of Near-Ultimate Strength for Multiwalled Carbon Nanotubes and Irradiation-Induced Crosslinking Improvements. *Nat. Nanotechnol.* **2008**, *3*, 626–631.
3. Koziol, K.; Vilatela, J.; Moisala, A.; Motta, M.; Cunniff, P.; Sennett, M.; Windle, A. High-Performance Carbon Nanotube Fiber. *Science* **2007**, *318*, 1892–1895.
4. Motta, M.; Moisala, A.; Kinloch, I. A.; Windle, A. H. High Performance Fibres from 'Dog Bone' Carbon Nanotubes. *Adv. Mater.* **2007**, *19*, 3721–3726.
5. Vilatela, J. J.; Windle, A. H. Yarn-Like Carbon Nanotube Fibers. *Adv. Mater.* **2010**, *22*, 4959–4963.
6. Dalton, A. B.; Collins, S.; Muñoz, E.; Razal, J. M.; Ebron, V. H.; Ferraris, J. P.; Coleman, J. N.; Kim, B. G.; Baughman, R. H. Super-Tough Carbon-Nanotube Fibres. *Nature* **2003**, *423*, 703.
7. Miaudet, P.; Badaire, S.; Maugey, M.; Derre, A.; Pichot, V.; Launois, P.; Poulin, P.; Zakri, C. Hot-Drawing of Single and Multiwall Carbon Nanotube Fibers for High Toughness and Alignment. *Nano Lett.* **2005**, *5*, 2212–2215.
8. Behabtu, N.; Green, M. J.; Pasquali, M. Carbon Nanotube-Based Neat Fibers. *Nano Today* **2008**, *3*, 24–34.
9. Zhang, X.; Li, Q.; Holesinger, T. G.; Arendt, P. N.; Huang, J.; Kirven, P. D.; Clapp, T. G.; DePaula, R. F.; Liao, X.; Zhao, Y.; *et al.* Ultrastrong, Stiff, and Lightweight Carbon-Nanotube Fibers. *Adv. Mater.* **2007**, *19*, 4198–4201.
10. Zhang, X.; Li, Q.; Tu, Y.; Li, Y.; Coulter, J. Y.; Zheng, L.; Zhao, Y.; Jia, Q.; Peterson, D. E.; Zhu, Y. Strong Carbon-Nanotube Fibers Spun from Long Carbon-Nanotube Arrays. *Small* **2007**, *3*, 244–248.
11. Tran, C. D.; Humphries, W.; Smith, S. M.; Huynh, C.; Lucas, S. Improving the Tensile Strength of Carbon Nanotube Spun Yarns Using a Modified Spinning Process. *Carbon* **2009**, *47*, 2662–2670.
12. Liu, K.; Sun, Y.; Lin, X.; Zhou, R.; Wang, J.; Fan, S.; Jiang, K. Scratch-Resistant, Highly Conductive, and High-Strength Carbon Nanotube-Based Composite Yarns. *ACS Nano* **2010**, *4*, 5827–5834.
13. Miao, M.; McDonnell, J.; Vuckovic, L.; Hawkins, S. C. Poisson's Ratio and Porosity of Carbon Nanotube Dry-Spun Yarns. *Carbon* **2010**, *48*, 2802–2811.
14. Randeniya, L. K.; Bendavid, A.; Martin, P. J.; Tran, C.-D. Composite Yarns of Multiwalled Carbon Nanotubes with Metallic Electrical Conductivity. *Small* **2010**, *6*, 1806–1811.
15. Miao, M. Electrical Conductivity of Pure Carbon Nanotube Yarns. *Carbon* **2011**, *49*, 3755–3761.
16. Ryu, S.; Lee, Y.; Hwang, J.-W.; Hong, S.; Kim, C.; Park, T. G.; Lee, H.; Hong, S. H. High-Strength Carbon Nanotube Fibers Fabricated by Infiltration and Curing of Mussel-Inspired Catecholamine Polymer. *Adv. Mater.* **2011**, *23*, 1971–1975.
17. Tran, C.-D.; Lucas, S.; Phillips, D. G.; Randeniya, L. K.; Baughman, R. H.; Tran-Cong, T. Manufacturing Polymer/Carbon Nanotube Composite Using a Novel Direct Process. *Nanotechnology* **2011**, *22*, 145302.
18. Ma, W.; Liu, L.; Zhang, Z.; Yang, R.; Liu, G.; Zhang, T.; An, X.; Yi, X.; Ren, Y.; Niu, Z.; et al. High-Strength Composite Fibers: Realizing True Potential of Carbon Nanotubes in Polymer Matrix through Continuous Reticulate Architecture and Molecular Level Couplings. *Nano Lett.* **2009**, *9*, 2855–2861.
19. Naraghi, M.; Filleter, T.; Moravsky, A.; Locascio, M.; Loutfy, R. O.; Espinosa, H. D. A Multiscale Study of High Performance Double-Walled Nanotube–Polymer Fibers. *ACS Nano* **2010**, *4*, 6463–6476.
20. Treacy, M. M. J.; Ebbesen, T. W.; Gibson, J. M. Exceptionally High Young's Modulus Observed for Individual Carbon Nanotubes. *Nature* **1996**, *381*, 678–680.
21. Yu, M.-F.; Files, B. S.; Arepalli, S.; Ruoff, R. S. Tensile Loading of Ropes of Single Wall Carbon Nanotubes and their Mechanical Properties. *Phys. Rev. Lett.* **2000**, *84*, 5552–5555.
22. Demczyk, B.; Wang, Y. M.; Cumings, J.; Hetman, M.; Han, W.; Zettl, A.; Ritchie, R. O. Direct Mechanical Measurement of the Tensile Strength and Elastic Modulus of Multiwalled Carbon Nanotubes. *Mater. Sci. Eng., A* **2002**, *334*, 173–178.
23. Boncel, S.; Sundaram, R. M.; Windle, A. H.; Koziol, K. K. Enhancement of the Mechanical Properties of Directly

Spun CNT Fibers by Chemical Treatment. *ACS Nano* **2011**, *5*, 9339–9344.
24. Beese, A. M.; Sarkar, S.; Nair, A.; Naraghi, M.; An, Z.; Moravsky, A.; Loutfy, R. O.; Buehler, M. J.; Nguyen, S. T.; Espinosa, H. D. Bio-Inspired Carbon Nanotube–Polymer Composite Yarns with Hydrogen Bond-Mediated Lateral Interactions. *ACS Nano* **2013**, *7*, 3434–3446.
25. Hearle, J. W. S.; Grosberg, P.; Backer, S. *Structural Mechanics of Fibers, Yarns, and Fabrics*; Wiley-Interscience: New York, 1969.
26. Naraghi, M.; Bratzel, G. H.; Filleter, T.; An, Z.; Wei, X.; Nguyen, S. T.; Buehler, M. J.; Espinosa, H. D. Atomistic Investigation of Load Transfer between DWNT Bundles "Crosslinked" by PMMA Oligomers. *Adv. Funct. Mater.* **2013**, *23*, 1883–1892.
27. Pitt, R. E.; Phoenix, S. L. On Modelling the Statistical Strength of Yarns and Cables Under Localized Load-Sharing among Fibers. *Text. Res. J.* **1981**, *51*, 408–425.
28. Porwal, P. K.; Beyerlein, I. J.; Phoenix, S. L. Statistical Strength of Twisted Fiber Bundles with Load Sharing Controlled by Frictional Length Scales. *J. Mech. Mater. Struct.* **2007**, *2*, 773–791.
29. Wei, X.; Naraghi, M.; Espinosa, H. D. Optimal Length Scales Emerging from Shear Load Transfer in Natural Materials: Application to Carbon-Based Nanocomposite Design. *ACS Nano* **2012**, *6*, 2333–2344.
30. Gao, H.; Ji, B.; Jäger, I. L.; Arzt, E.; Fratzl, P. Materials Become Insensitive to Flaws at Nanoscale: Lessons from Nature. *Proc. Natl. Acad. Sci. U.S.A.* **2003**, *100*, 5597–5600.
31. Espinosa, H. D.; Rim, J. E.; Barthelat, F.; Buehler, M. J. Merger of Structure and Material in Nacre and Bone–Perspectives on De Novo Biomimetic Materials. *Prog. Mater. Sci.* **2009**, *54*, 1059–1100.
32. Espinosa, H. D.; Juster, A. L.; Latourte, F. J.; Loh, O. Y.; Gregoire, D.; Zavattieri, P. D. Tablet-Level Origin of Toughening in Abalone Shells and Translation to Synthetic Composite Materials. *Nat. Commun.* **2011**, *2*, 173.
33. Chen, B.; Wu, P. D.; Gao, H. A Characteristic Length for Stress Transfer in the Nanostructure of Biological Composites. *Compos. Sci. Technol.* **2009**, *69*, 1160–1164.
34. Barthelat, F.; Dastjerdi, A. K.; Rabiei, R. An Improved Failure Criterion for Biological and Engineered Staggered Composites. *J. R. Soc., Interface* **2013**, *10*, 20120849.
35. Filleter, T.; Bernal, R.; Li, S.; Espinosa, H. D. Ultrahigh Strength and Stiffness in Cross-Linked Hierarchical Carbon Nanotube Bundles. *Adv. Mater.* **2011**, *23*, 2855–2860.
36. Behabtu, N.; Young, C. C.; Tsentalovich, D. E.; Kleinerman, O.; Wang, X.; Ma, A. W. K.; Bengio, E. A.; ter Waarbeek, R. F.; de Jong, J. J.; Hoogerwerf, R. E.; *et al.* Strong, Light, Multifunctional Fibers of Carbon Nanotubes with Ultrahigh Conductivity. *Science* **2013**, *339*, 182–186.
37. Yu, M.-F.; Lourie, O.; Dyer, M. J.; Moloni, K.; Kelly, T. F.; Ruoff, R. S. Strength and Breaking Mechanism of Multiwalled Carbon Nanotubes Under Tensile Load. *Science* **2000**, *287*, 637–640.
38. Schrauwen, B. A. G.; v. Breemen, L. C. A.; Spoelstra, A. B.; Govaert, L. E.; Peters, G. W. M.; Meijer, H. E. H. Structure, Deformation, and Failure of Flow-Oriented Semicrystalline Polymers. *Macromolecules* **2004**, *37*, 8618–8633.
39. Giboz, J.; Spoelstra, A. B.; Portale, G.; Copponnex, T.; Meijer, H. E. H.; Peters, G. W. M.; Méle, P. On the Origin of the "Core-Free" Morphology in Microinjection-Molded HDPE. *J. Polym. Sci., Part B: Polym. Phys.* **2011**, *49*, 1470–1478.
40. Lu, W.; Zu, M.; Byun, J.-H.; Kim, B.-S.; Chou, T.-W. State of the Art of Carbon Nanotube Fibers: Opportunities and Challenges. *Adv. Mater.* **2012**, *24*, 1805–1833.
41. Chen, X.; Zheng, M.; Park, C.; Ke, C. Direct Measurements of the Mechanical Strength of Carbon Nanotube–Poly (methyl methacrylate) Interfaces. *Small* **2013**, *9*, 3345–3351.
42. Paci, J. T.; Furmanchuk, A.; Espinosa, H. D.; Schatz, G. C. Shear and Friction between Carbon Nanotubes in Bundles and Yarns. *Nano Lett.* **2014**, 10.1021/nl502210r.
43. Filleter, T.; Espinosa, H. D. Multi-Scale Mechanical Improvement Produced in Carbon Nanotube Fibers by Irradiation Cross-Linking. *Carbon* **2013**, *56*, 1–11.